Supplemental Material for *Anisotropic magnetic interactions in a candidate Kitaev spin liquid close to a metal-insulator transition*

Supplementary Note 1. Details on theoretical calculations

Extended Kitaev Hamiltonian. We consider the effective spin-$\frac{1}{2}$ extended Kitaev Hamiltonian on the honeycomb lattice with exchanges on up to $n = 3$rd-neighbor bonds:

$$\begin{aligned} H = \quad & \sum_{n=1}^{3} \sum_{\langle ij \rangle_n} J_n \, \mathbf{S}_i \cdot \mathbf{S}_j + K_n \, S_i^{\gamma} S_j^{\gamma} + \Gamma_n \left(S_i^{\alpha} S_j^{\beta} + S_i^{\beta} S_j^{\alpha} \right) \\ & + \Gamma_n' \left(S_i^{\gamma} S_j^{\alpha} + S_i^{\gamma} S_j^{\beta} + S_i^{\alpha} S_j^{\gamma} + S_i^{\beta} S_j^{\gamma} \right) - \mu_0 \mu_{\mathrm{B}} \sum_i \mathbf{H} \cdot \mathbb{G} \cdot \mathbf{S}_i \end{aligned} \tag{1}$$

Here, canonical X_n, Y_n and Z_n bonds are defined for nth-nearest-neighbors according to their orientation in the honeycomb lattice (see, e.g., Ref. [1]). Then, in Eq. (1), $(\alpha, \beta, \gamma) = (x, y, z)$ for Z_n-bonds, $(\alpha, \beta, \gamma) = (y, z, x)$ for X_n-bonds and $(\alpha, \beta, \gamma) = (z, x, y)$ for Y_n-bonds. The last term in Eq. (1) represents the Zeeman coupling to an external magnetic field $\mathbf{H}$, through the anisotropic g-tensor $\mathbb{G}$. We compute thermodynamic properties in these models using the orthogonalized finite-temperature Lanczos method (OFTLM) [2] as described in the method section of the main text.

Fully *ab-initio* model. We first considered the fully-*ab-initio* computed model for $\mathrm{RuI_3}$ of Ref. [3]. Here, the exchange couplings are $(J_1, K_1, \Gamma_1, \Gamma_1', J_2, K_2, \Gamma_2, \Gamma_2', J_3, K_3, \Gamma_3, \Gamma_3') \approx (-0.1, -5.8, -0.7, -1.9, 0.5, -1.1, 0.6, 0.2, -0.1, 0.3, 0, -0.2)\,\mathrm{meV}$ and the in-plane (out-of-plane) g-value is $g_{ab} = 2.3$ ($g_c = 1.8$). This model in our OFTLM calculations captures various key features of the torque measurements: A six-fold periodic torque in the ab-plane and in the b^*c-plane a saw-tooth anisotropic torque at low temperatures, that, upon increasing temperature, evolves into one with a sinusoidal θ-dependence and changes sign at higher temperatures. These described features fit the experimentally observed behavior well. However, the respective absolute sign differs from experiment, i.e., in this model, the temperature-induced switch of anisotropy is from effective easy-axis (low temperature) to easy-plane (high temperature).

Adjusted model. As most of the qualitative features of the torque measurements can be reproduced with the aforementioned exchange parameters, we opt to phenomenologically adjust the *ab-initio* parameters in order to reproduce the absolute sign of torque. The degree of easy-plane anisotropy of the exchange interactions, which influence primarily the low-temperature torque, can be classically estimated by $E_c - E_{ab} \propto \Gamma_1 + 2\Gamma_1' + 2\Gamma_2 + 4\Gamma_2' + \Gamma_3 + 2\Gamma_3'$, where E_c (E_{ab}) is the energy of the state fully polarized along c (ab) for given parameters. A positive (negative) $E_c - E_{ab}$ then indicates an easy-ab-plane (easy-c-axis) exchange. As longer-range interactions become more important for heavier ligands, and longer-range interactions are at the same time expected to be potentially underestimated in the two-site method of Ref. [3], we consider an adjustment of the easy-plane anisotropy $E_c - E_{ab}$ by increasing as a representative for the anisotropic longer-range exchanges the second-neighbor anisotropic exchange Γ_2' by 2 meV. While this changes the model's ground state from a quantum-disordered one to a ferromagnetic one, we note that the ground state in the original model is sensitive to small changes in the exchange parameters, the qualitative saw-tooth torque behavior is less fragile, and appears to be primarily governed by $E_c - E_{ab}$, which becomes positive upon the increase of Γ_2'. To reproduce the experimentally observed high-temperature sign of torque, we set the effective g-values as $g_{ab} = 1.8$ and $g_c = 2.3$.

We therefore consider the following *adjusted* version of the fully-*ab-initio* computed model for $\mathrm{RuI_3}$ of Ref. [3]: $(J_1, K_1, \Gamma_1, \Gamma_1', J_2, K_2, \Gamma_2, \Gamma_2', J_3, K_3, \Gamma_3, \Gamma_3') \approx (-0.1, -5.8, -0.7, -1.9, 0.5, -1.1, 0.6, \mathbf{2.2}, -0.1, 0.3, 0, -0.2)\,\mathrm{meV}$ and an in-plane (out-of-plane) g-value of $g_{ab} = \mathbf{1.8}$ ($g_c = \mathbf{2.3}$). Highlighted as bold are those values that are adjusted from the *ab-initio* values of Ref. [3]. The OFTLM results for these model parameters are presented in Fig. 1 and Fig. 3e,f,i of the main text. Figs. 1(a),(b) show the torque for rotation in the b^*c-plane at high and low temperatures, where the saw-tooth dependence gradually develops below $\sim$30 K, as observed in experiment. The temperature-induced reversal from easy-plane to easy-axis anisotropy can be diagnosed both from the sign change of torque at $\sim$95 K (Fig. 1(a)) and the crossing of in-plane and out-of-plane magnetic susceptibilities at this temperature (Fig. 1(d)). Fig. 1(c) shows the torque for rotation in the ab-plane, which shows six-fold periodicity and indicates b^* as the stable equilibrium direction.

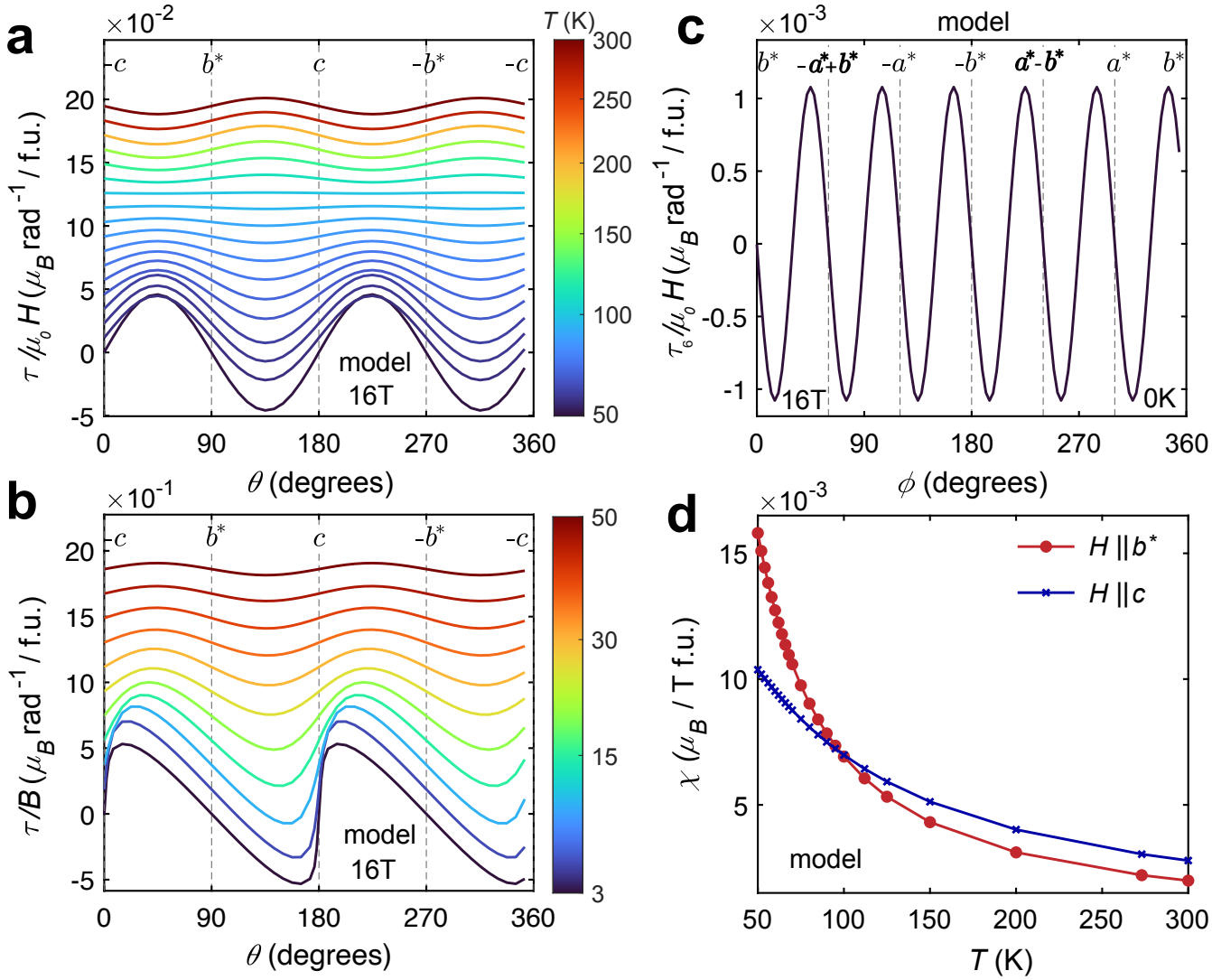

Supplementary Figure 1. Theoretical modelling of RuI_3. (a) Torque at 16 T as a function of magnetic field orientation in the b^*c plane. Curves are vertically offset for clarity, colour-coded by temperature decreasing from 300 K to 50 K. (b) Same as (a) but for the low-temperature range 2 to 50 K. (c) Zero-temperature torque for field in the ab plane indicating a six-fold periodicity with a stable equilibrium position for in-plane field along the b^* axis (parallel to a Ru-Ru bond). Top labels and vertical lines show when the applied field is parallel to reference crystallographic directions. (d) Calculated temperature-dependence of the magnetic susceptibility for field along the b^* (filled circles) and c (crosses) directions, which intersect near $T^* \simeq 95$ K. (a), (b), and (c) are to be compared with experimental data in Fig. 3 (a), (b), and (d) respectively.

Supplementary Note 2. Additional experimental data and parametrization of torque data

Structural analysis

We present additional experimental data and extract various parameters to strengthen the findings in the main manuscript. Fig. 2 shows in detail the X-ray data for different reflections planes for two un-twinned single crystals of α-RuI_3.

Temperature-dependent torque studies

The complete temperature dependence torque data measured for three different directions of the applied magnetic field in relation to the honeycomb plane in the case of sample S1 are shown in Fig. 3 whereas for the sample S2 are plotted in Fig. 8. All the angular dependent torque data were analyzed, as described in detailed in Methods, and the different extracted parameters related to the Fourier amplitudes and the sawtooth parameters as a function of temperature are shown in Fig. 4 for sample S1 and Fig. 9 for sample S2, respectively. The temperature dependence of the A_2 amplitude, corresponding to $\sin 2\theta$ term, is fitted to a Curie-Weiss like dependence, $A_2 = C^*/(T - \Theta_{\rm CW}) + A_{20}$ where A_{20} is an offset, in the temperature range 50 to 150 K and the extracted parameters are listed in Supplementary Table 1.

Field-dependent torque studies

Additionally, we have investigated the angular dependence of torque at two fixed temperatures as a function of magnetic field illustrated in Fig. 2 for sample S1 and Fig. 6. These data are also analyzed employing the same approach used above for the temperature dependence studies with the extracted parameters shown in Fig. 5 for sample S1 and in Fig. 7 for sample S2.

The field dependence of torque measured at fixed angles, θ at low temperatures ($T = 2$ or 3 K), enables to define a characteristic field, H^*, as the local maximum field of τ/H versus H. The angular dependence of H^* for different angles θ is used to extract anisotropic fields, H_c^* and H_{ab}^*, using an empirical anisotropic dependence, as described in Methods, and applied in Figs.4(d) and 10.

Supplementary Table 1. Parameters extracted from experimental torque data of α-RuI_3 for two different untwinned single crystals (S1 and S2). The values extracted from the temperature dependencies of the A_2 parameters are the temperature, T^*, at which the A_2 torque component changes sign, and the extracted Curie-Weiss temperature for a range between 50 to 150 K. The parameters extracted from the angular dependence of H^* field at low temperature are H_c^* and H_{ab}^*, using an empirical angular dependence for anisotropic systems, described in Methods.

Sample	Plane	T^*(K)	$\Theta_{\rm CW}$ (K)	H_c^* (T)	H_{ab}^* (T)
S1	ac	96 ± 1	-25.0 ± 4.2	11.1 ± 0.6	3.7 ± 0.3
	b^*c	95.6 ± 0.1	-24.2 ± 5.9	10.9 ± 0.6	3.8 ± 0.3
S2	bc	94 ± 5	-31.1	10.4 ± 1.0	3.9 ± 0.6
	a^*c	99 ± 4	-25.8	10.8 ± 0.6	4.0 ± 0.3

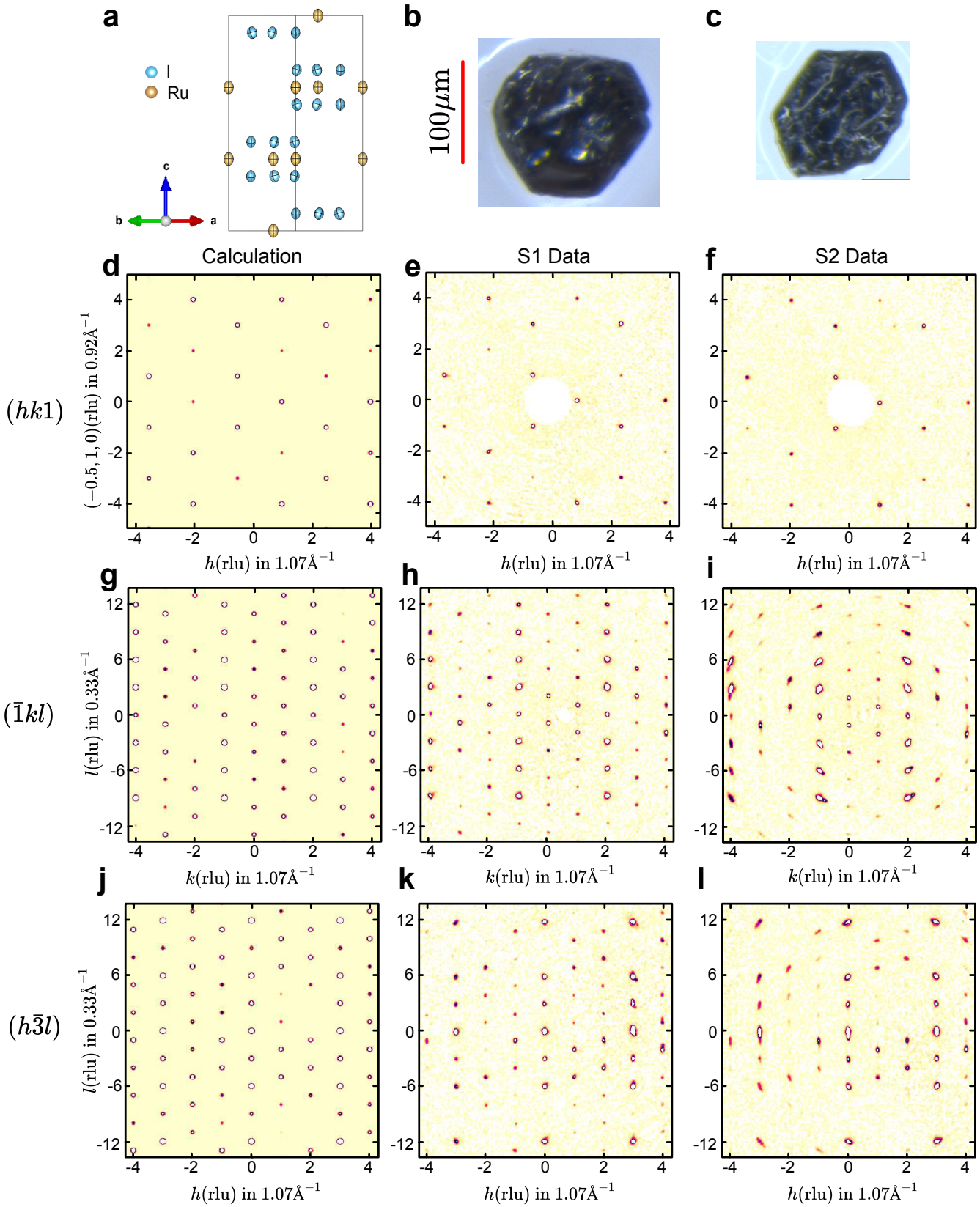

Supplementary Figure 2. Structural characterization of crystals. (a) The crystal structure obtained by refinement of the nominal $R\bar{3}$ structure of stoichiometric RuI_3 (fully occupied Ru $6c$ site) from Ref. [4], against the x-ray diffraction data of sample S1. The ellipsoids illustrate the fitted anisotropic displacement parameters. (b-c) Images of the S1 and S2 samples. (d-l) X-ray diffraction patterns in representative (hkl) planes: (d-f) $(hk1)$, (g-i) $(\bar{1}kl)$, and (j-l) $(h\bar{3}l)$. Left column is calculation for the nominal structure in (a); middle and right columns are data for samples S1 and S2, respectively.

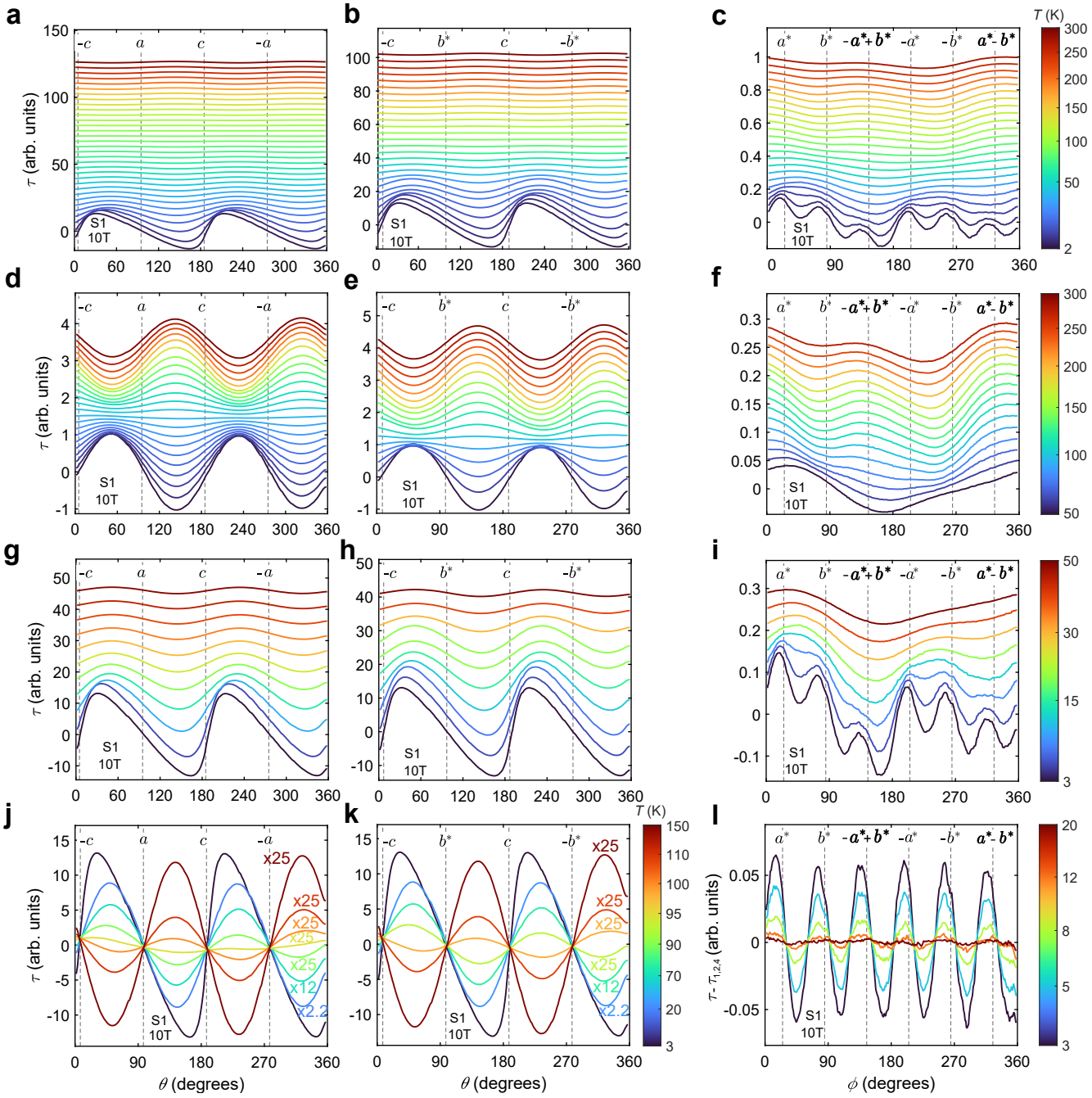

Supplementary Figure 3. Angular dependence of torque at different temperatures (2 to 300 K) in fixed magnetic field of 10 T for sample S1. Angular dependence of the torque over a large temperature range for three different sample orientations: $H \parallel ac$ (left column), $H \parallel b^*c$ (middle column), and $H \parallel ab$ (right column) with curves color coded by the measured temperature as per the right side colorbars. Different rows correspond to different temperature regimes: (a-c) full-temperature range (2 to 300 K), (d-f) high-temperature range (50 to 300 K), and (g-l) low-temperature range (2 to 50 K). Angular dependence for $H \parallel ac$ in (j) and $H \parallel b^*c$ in (k) emphasizes the sign change of torque around $T^* \simeq 95$ K. Curve are multiplied by different factors (as labelled) to bring them on the same scale. (l) Angular dependence of torque component for $H \parallel ab$ after subtracting the non-intrinsic contributions from the raw data, $\tau - \tau_{1,2,4}$. In each panel top axes labels and vertical dashed lines indicate when the field direction is along reference crystal axes in the rotation plane.

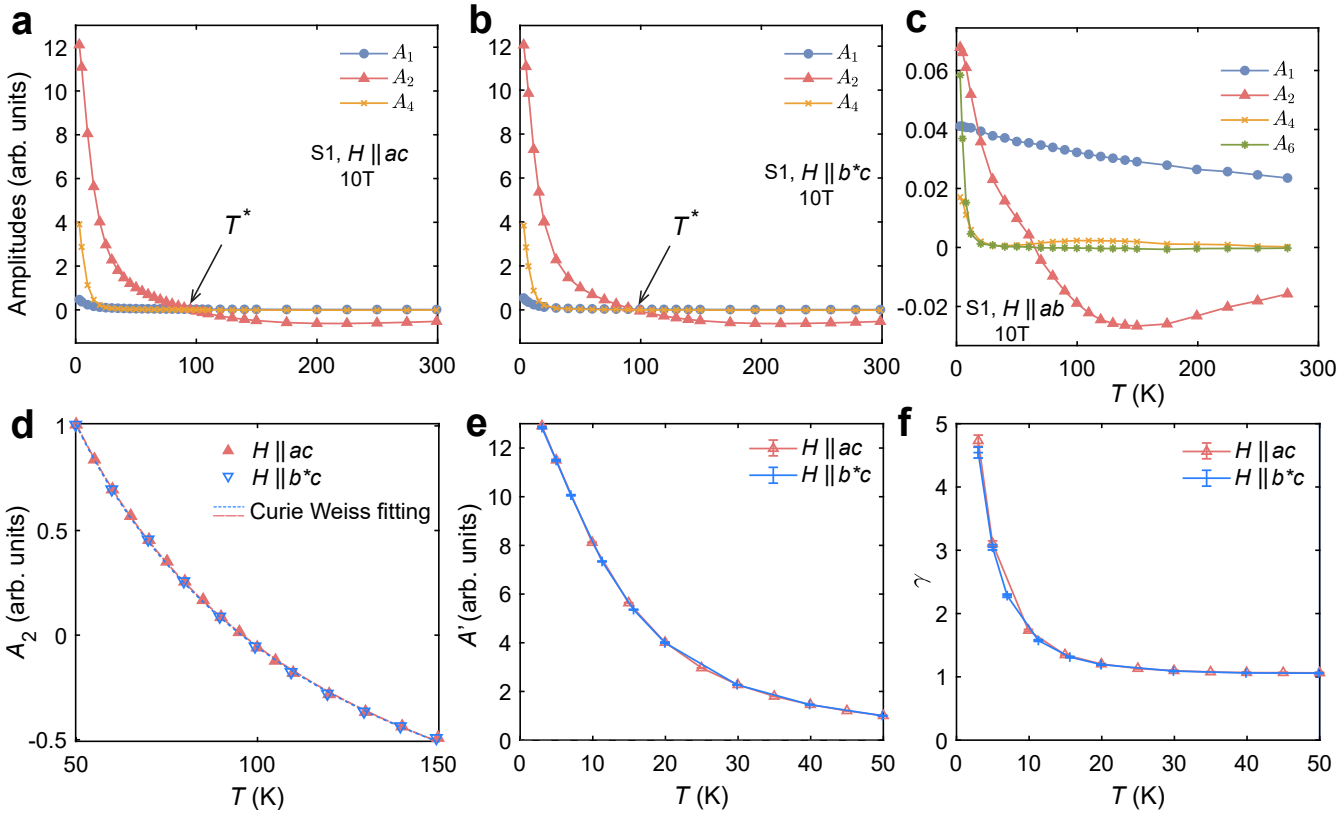

Supplementary Figure 4. Temperature dependence of fitted torque components extracted from the data in Fig. 3 for sample S1 at 10 T (a-c) A_1 (filled circles), A_2 (filled triangles) and A_4 (crosses) for $H \parallel ac$ shown in (a), for $H \parallel b^*c$ in (b), and additionally A_6 (stars) for $H \parallel ab$ in (c). (d) Curie-Weiss fit of the A_2 component for $H \parallel ac$ (filled up-triangles) and $H \parallel b^*c$ (empty down-triangles) in the temperature range 50 to 150 K (dashed lines). (e,f) Temperature dependence of the amplitude A' in (e) and the saw-tooth parameter γ in (f), extracted from fitting the measured torque to the empirical saw-tooth shape described in the text, in the low temperature range (2 to 50 K) for $H \parallel ac$ (triangles) and for $H \parallel b^*c$ (crosses). The error bars in all panels represent the 95% confidence interval in the fitted parameter values.

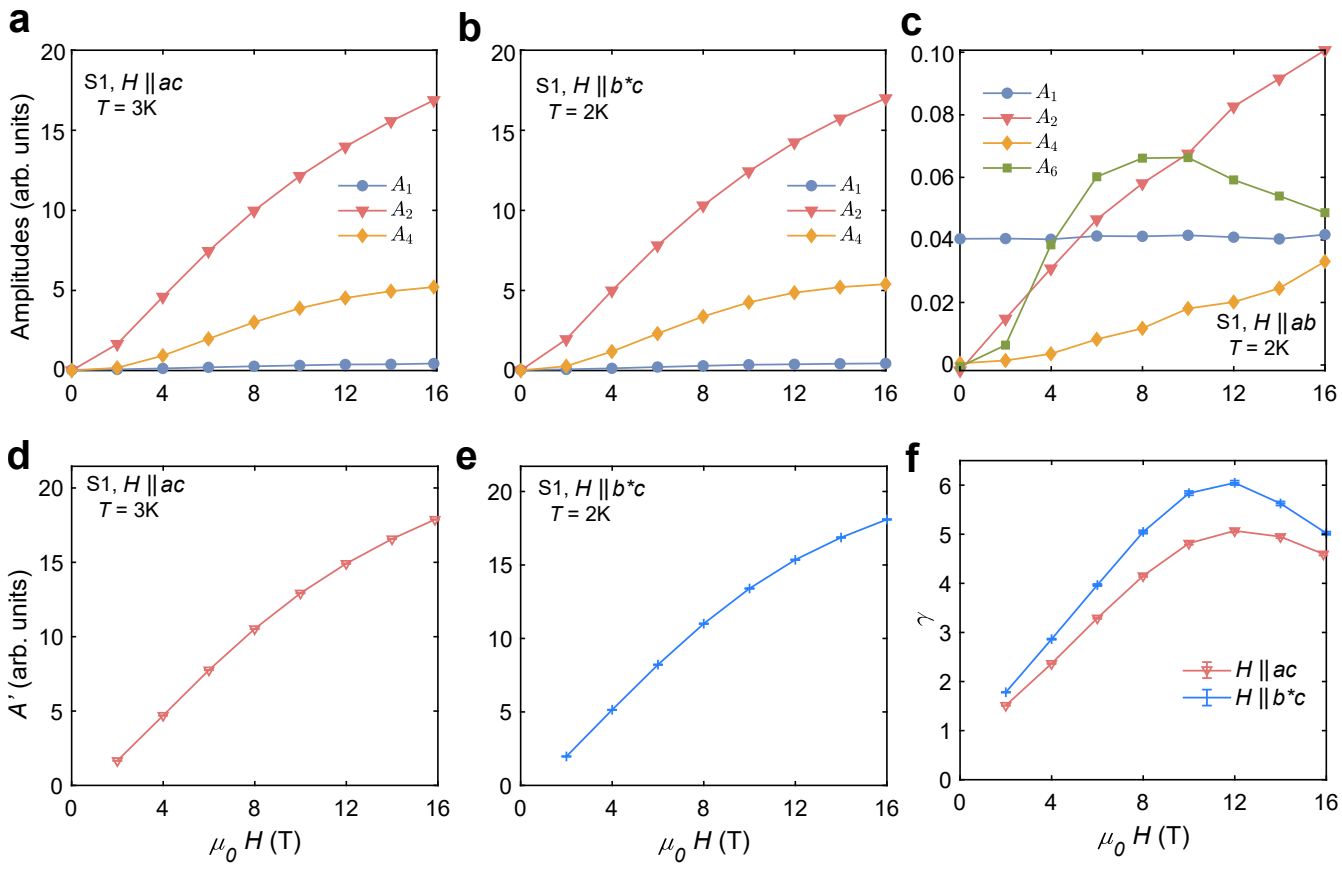

Supplementary Figure 5. Field dependence of the different torque components from the data in Fig. 2 for sample S1 at base temperature (2 or 3 K). (a-c) A_1 (filled circles), A_2 (filled triangles) and A_4 (filled diamonds) for $H \parallel ac$ shown in (a), for $H \parallel b^*c$ in (b), and additionally A_6 (solid square) for $H \parallel ab$ in (c). Field dependence of the amplitude A' in (d, e) and saw-tooth parameter γ in (f), extracted from fitting the measured torque to the empirical saw-tooth shape described in the text, for $H \parallel ac$ (empty triangles) and for $H \parallel b^*c$ (crosses). The error bars in all panels represent the 95% confidence interval in the fitted parameter values.

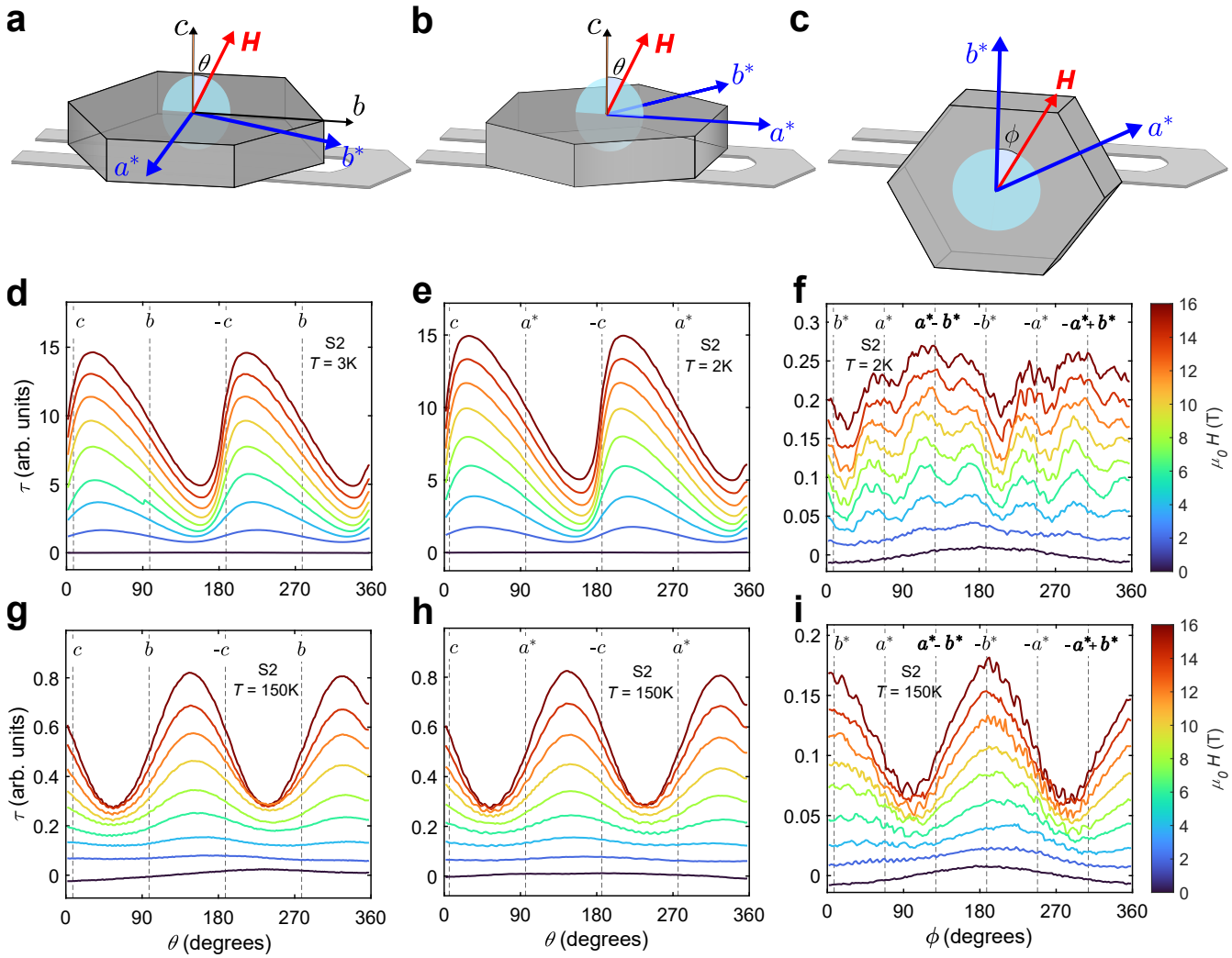

Supplementary Figure 6. Angular dependence of torque for field orientation in three orthogonal crystallographic planes, at different fixed temperature and various magnetic field strengths for sample S2 (a-c) Schematic diagram of the hexagonally-shaped sample mounted on the piezocantilever in three orientations. The light blue disk shows the plane in which the field orientation changes relative to the crystal axes. (a,b) $\theta = 0°$ is close to $H \parallel c$ and in (c) $\phi = 0°$ is close to $H \parallel b^*$. (d-i) Angular dependence of torque for fixed field strength increasing from bottom (0 T) to top (16 T)), with curves offset vertically for clarity and colour-coded in the right-hand colorbars. Top axes labels and vertical dashed lines indicate when the field direction is along reference crystal axes in the rotation plane. Bottom row shows data at high temperature (150 K) and middle row at base temperature (2 or 3 K).

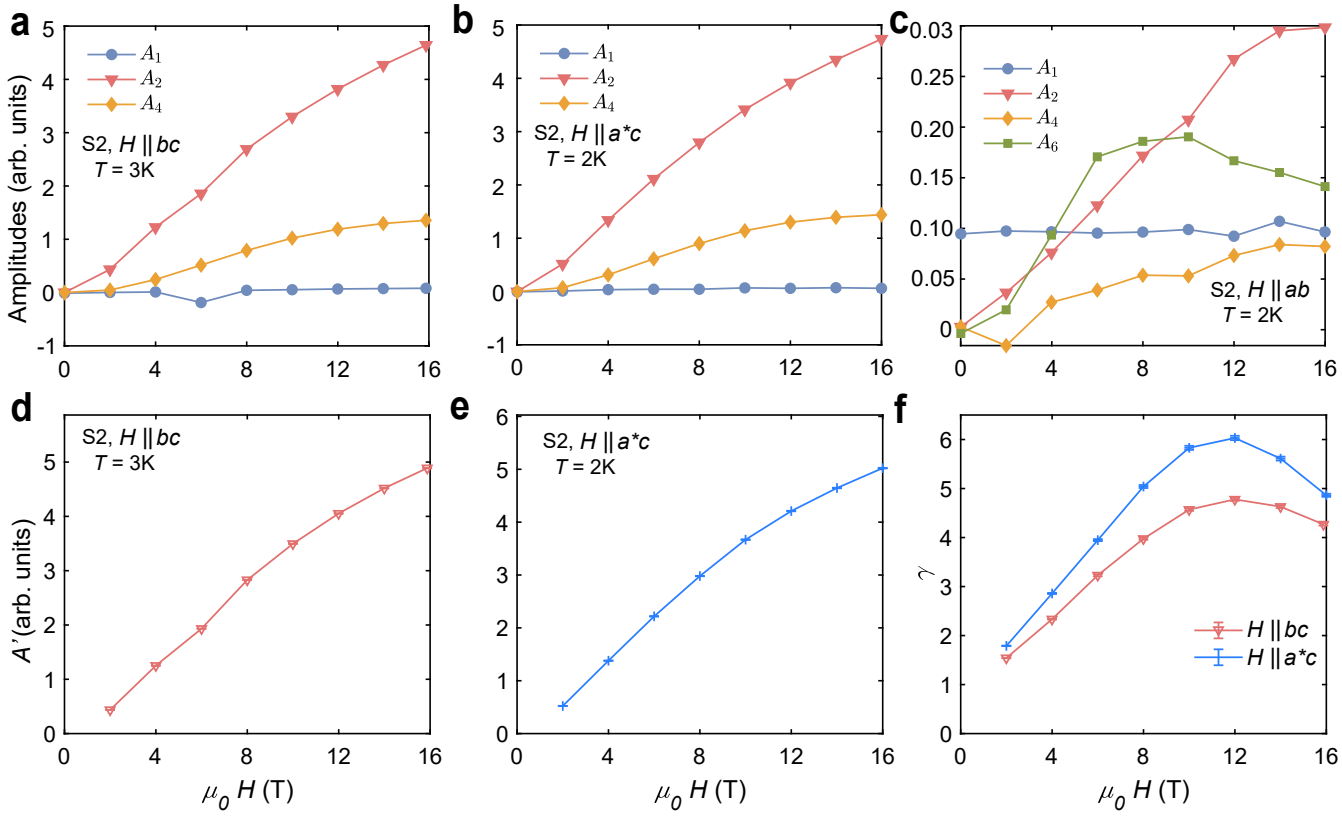

Supplementary Figure 7. Field dependence of the different torque components extracted from the data in Supplementary Fig. 6 at base temperature (2 or 3 K). (a-c) A_1 (filled circles), A_2 (filled triangles) and A_4 (filled diamonds) for $H \parallel bc$ shown in (a), for $H \parallel a^*c$ in (b), and additionally A_6 (solid square) for $H \parallel ab$ in (c). Field dependence of the amplitude A' in (d, e) and saw-tooth parameter γ in (f), extracted from fitting the measured torque to the empirical saw-tooth shape described in the text, for $H \parallel bc$ (empty triangles) and for $H \parallel a^*c$ (crosses). The error bars in all panels indicate the 95% confidence interval in the the fitted parameter values.

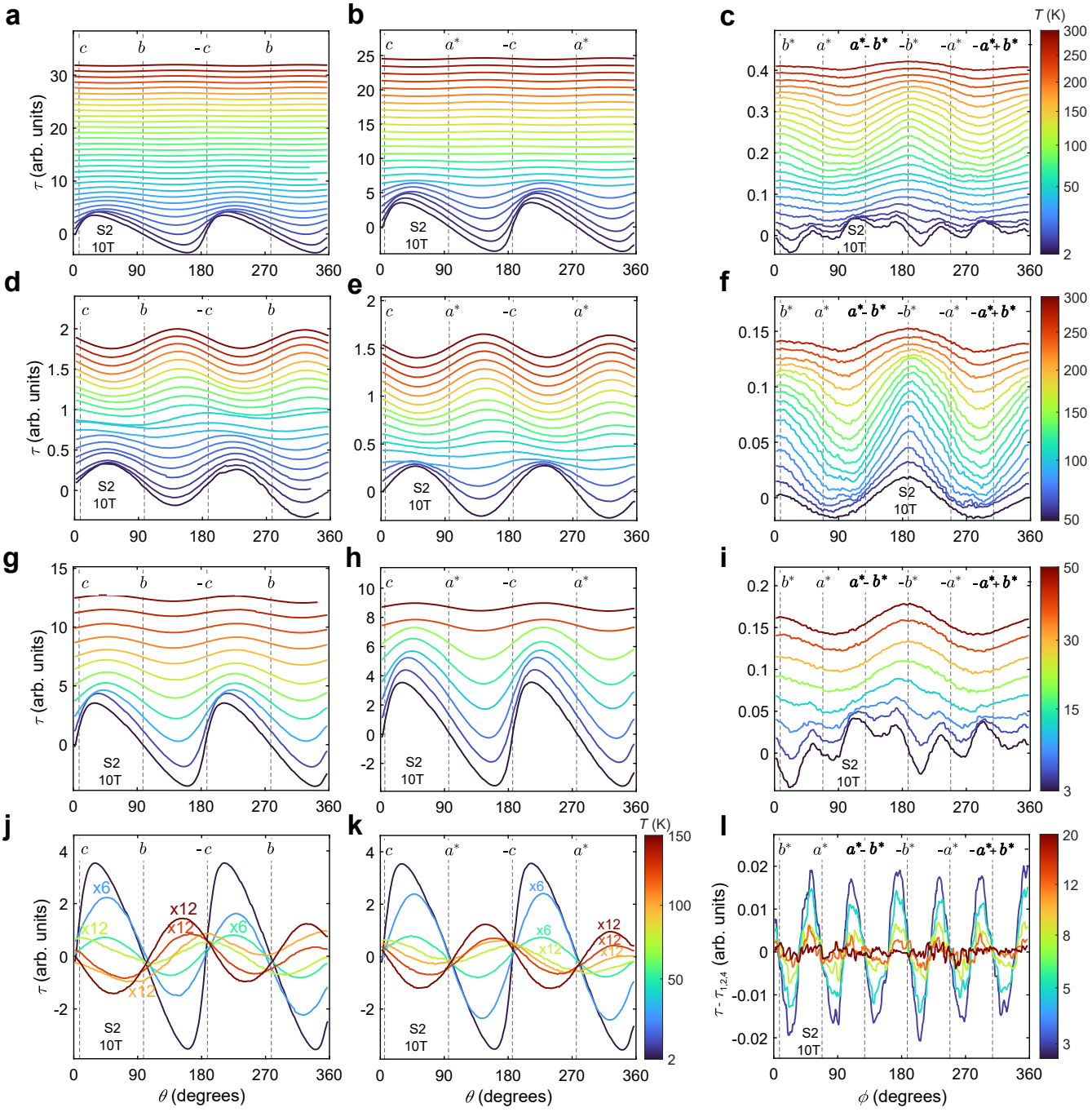

Supplementary Figure 8. Angular dependence of torque at different temperatures (2 to 300 K) in fixed magnetic field of 10 T for sample S2. Angular dependence of the torque over a large temperature range for three different sample orientations: $H \parallel bc$ (left column), $H \parallel a^*c$ (middle column), and $H \parallel ab$ (right column) with curves color coded by the measured temperature as per the right side colorbars. Different rows correspond to different temperature regimes: (a-c) full-temperature range (2 to 300 K), (d-f) high-temperature range (50 to 300 K), and (g-l) low-temperature range (2 to 50 K). Angular dependence for $H \parallel bc$ in (j) and $H \parallel a^*c$ in (k) emphasizes the sign change of torque around $T^* \simeq 95$ K. Curve are multiplied by different factors (as labelled) to bring them on the same scale. (l) Angular dependence of torque component for $H \parallel ab$ after subtracting the non-intrinsic contributions from the raw data, $\tau - \tau_{1,2,4}$. In each panel top axes labels and vertical dashed lines indicate when the field direction is along reference crystal axes in the rotation plane.

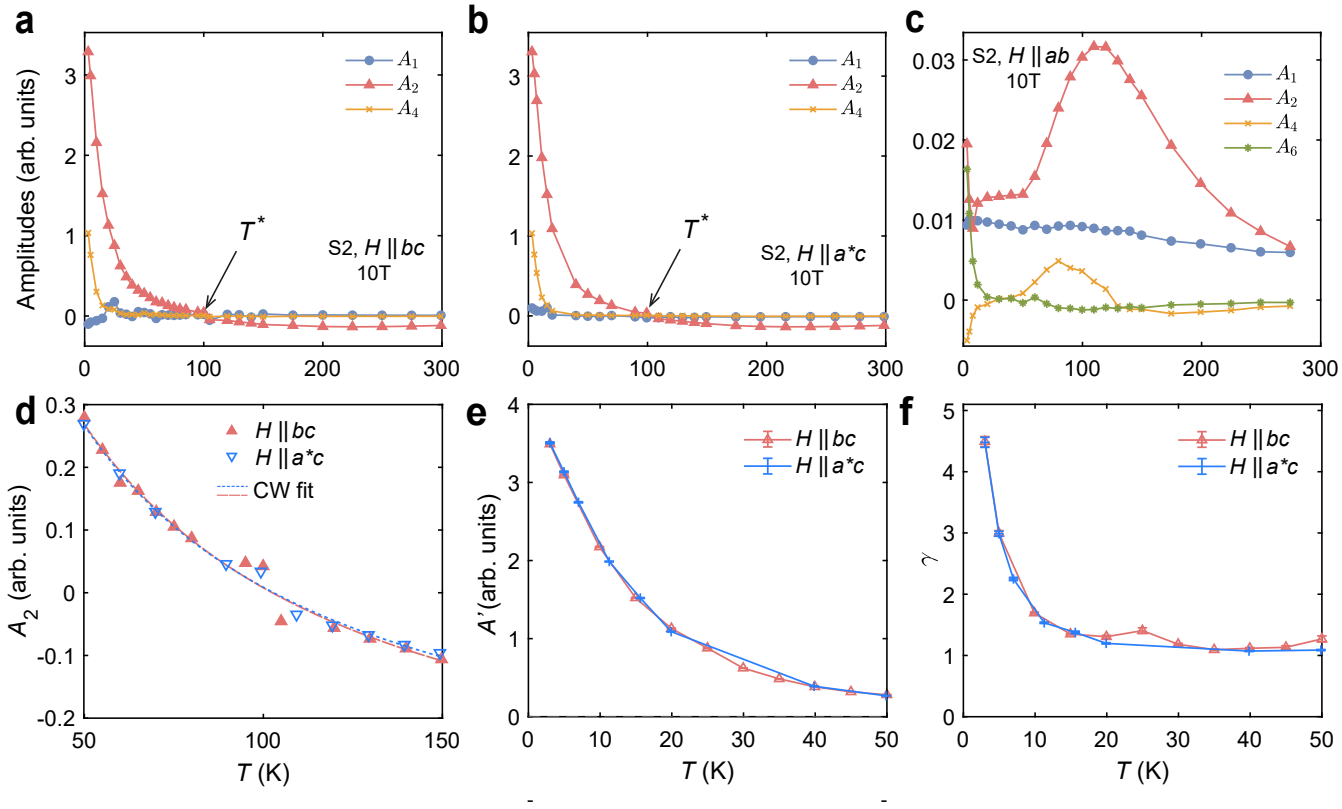

Supplementary Figure 9. Temperature dependence of different torque components extracted from the data in Supplementary Fig. 8 at 10 T. (a-c) A_1 (filled circles), A_2 (filled triangles) and A_4 (crosses) for $H \parallel bc$ shown in (a), for $H \parallel a^*c$ in (b), and additionally A_6 (stars) for $H \parallel ab$ in (c). (d) Curie-Weiss fit of the A_2 component for $H \parallel bc$ (filled up-triangles) and $H \parallel a^*c$ (empty down-triangles) in the temperature range 50 to 150 K (dashed lines). (e,f) Temperature dependence of the amplitude A' in (e) and saw-tooth parameter γ in (f), extracted from fitting the measured torque to the empirical saw-tooth shape described in the text, in the low temperature range (2 to 50 K) for $H \parallel bc$ (empty up-triangles) and for $H \parallel a^*c$ (crosses). The error bars in all panels represent the 95% confidence interval in the fitted parameter values.

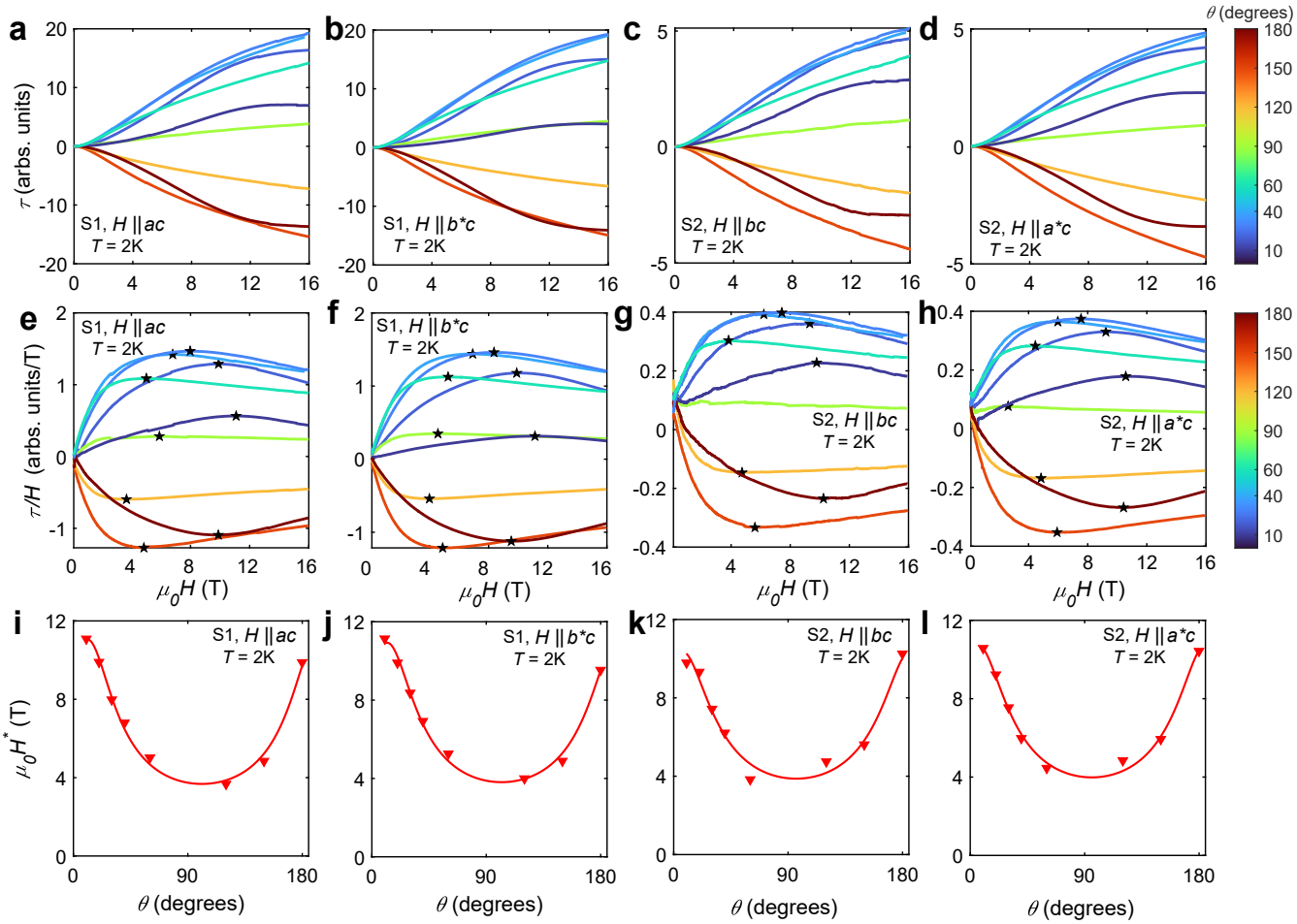

Supplementary Figure 10. Field dependence of the magnetic torque for different orientations and samples at $T = 2$ K. (a-d) Torque τ against magnetic field H and (e-h) τ/H versus H with a local maximum at a field H^* (filled stars) (i-l). Angular dependence of H^*, solid curves are fits to the empirical Ginzburg-Landau form described in the Methods with fitting parameters listed in Table 1.

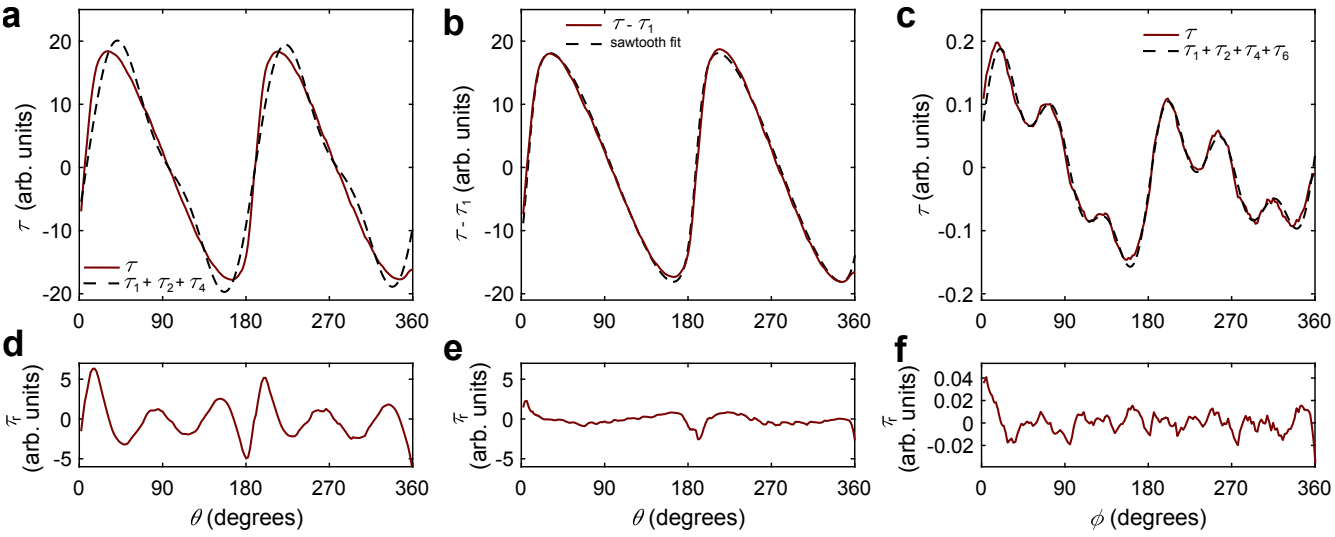

Supplementary Figure 11. Comparison between the different approaches used to extract torque amplitudes at 2 K and 16 T for sample S1. The Fourier transform with additional terms for $H||b^*c$ in (a) and for $H||ab$ in (c) or using an empirical fitting of the amplitude signal which captures the saw-tooth shape for $H||b^*c$ in (b), as detailed in Methods. The corresponding residuals, $\tau_r = \tau - \tau_{fit}$, are shown in the bottom row.

Supplementary References

References

[1] Winter, S. M., Li, Y., Jeschke, H. O. & Valentí, R. Challenges in design of Kitaev materials: Magnetic interactions from competing energy scales. *Phys. Rev. B* **93**, 214431 (2016). URL https://link.aps.org/doi/10.1103/PhysRevB.93.214431.

[2] Morita, K. & Tohyama, T. Finite-temperature properties of the Kitaev-Heisenberg models on kagome and triangular lattices studied by improved finite-temperature Lanczos methods. *Phys. Rev. Res.* **2**, 013205 (2020). URL https://link.aps.org/doi/10.1103/PhysRevResearch.2.013205.

[3] Kaib, D. A. S. *et al.* Electronic and magnetic properties of the RuX_3 (X=Cl, Br, I) family: two siblings and a cousin . *npj Quantum Mater.* **7**, 75 (2022). URL https://doi.org/10.1038/s41535-022-00481-3.

[4] Ni, D., Gui, X., Powderly, K. M. & Cava, R. J. Honeycomb-structure RuI_3, a new quantum material related to α-$RuCl_3$. *Adv. Mater.* **34**, 2106831 (2022). URL https://doi.org/10.1002/adma.202106831.